

Mid-infrared Imaging of a Circumstellar Disk Around HR 4796:
Mapping the Debris of Planetary Formation

D.W. Koerner^{1,2}, M.E. Ressler¹, M.W. Werner¹, and D.E. Backman³

Received _____; accepted _____

¹Jet Propulsion Laboratory, California Institute of Technology, 4800 Oak Grove Dr., Pasadena, CA 91109

²University of Pennsylvania, 4N14 DRL, 209 S. 33rd St., Philadelphia, PA 19104-6396

³Franklin & Marshall College, Dept. of Physics & Astronomy, PO Box 3003, Lancaster, PA 17604-3003

ABSTRACT

We report the discovery of a circumstellar disk around the young A0 star, HR 4796, in thermal infrared imaging carried out at the W.M. Keck Observatory. By fitting a model of the emission from a flat dusty disk to an image at $\lambda = 20.8 \mu\text{m}$, we derive a disk inclination, $i = 72^{\circ}_{-9^{\circ}}^{+6^{\circ}}$ from face on, with the long axis of emission at PA $28^{\circ} \pm 6^{\circ}$. The intensity of emission does not decrease with radius as expected for circumstellar disks but *increases* outward from the star, peaking near both ends of the elongated structure. We simulate this appearance by varying the inner radius in our model and find an inner hole in the disk with radius $R_{in} = 55 \pm 15$ AU. This value corresponds to the radial distance of our own Kuiper belt and may suggest a source of dust in the collision of cometesimals. By contrast with the appearance at $20.8 \mu\text{m}$, excess emission at $\lambda = 12.5 \mu\text{m}$ is faint and concentrated at the stellar position. This component is also detected in residual subtraction of the best-fit model from the $20.8 \mu\text{m}$ image. The intensity and ratio of flux densities at the two wavelengths could be accounted for by a tenuous dust component that is confined within a few AU of the star with mean temperature of a few hundred degrees K, similar to that of Zodiacal dust in our own solar system. The morphology of dust emission from HR 4796 (age 10 Myr) suggests that its disk is in a transitional planet-forming stage, between that of massive gaseous proto-stellar disks and more tenuous debris disks such as the one detected around Vega.

1. Introduction

It is now well over a decade since coronagraphic imaging of stellar light scattered by a disk around β Pictoris provided circumstantial evidence for the presence of an extra-solar planetary system (Smith & Terrile 1984). Since then, coronagraphic and adaptive-optics (AO) searches have continued the quest for additional examples (Smith, Fountain, & Terrile 1992; Kalas & Jewitt 1995), but none have been successful at imaging light scattered by dust around similar IRAS-selected candidates (see Table VII from Backman & Paresce 1993, for example). This failure was originally interpreted to suggest that the disk around β Pic is highly unusual (Smith & Terrile 1992), but subsequent identification of a few other main sequence A stars with fractional infrared excesses of the same magnitude has been used to argue that $\sim 20\%$ of all A-type stars pass through an early phase like that of β Pic (Jura et al. 1998). If true, the failure to image other candidates is likely due to their greater distance; limitations in current coronagraphic techniques would prevent detection of even β Pic's disk if it were several times farther away (cf. Kalas & Jewitt 1996). An alternative approach is suggested by successful imaging of the thermal dust emission from the disk around β Pic at mid-infrared wavelengths (Lagage & Pantin 1994; Pantin, Lagage, & Artymowicz 1997). As part of an effort to take full advantage of this technique, we present thermal infrared imaging of the circumstellar environment of HR 4796, a more distant A0 star (Houk 1982) suggested to have a disk similar to that of β Pic on the basis of its IRAS excess (Jura 1991; Jura et al. 1993; 1995; 1998).

At a distance of 67 ± 3 pc ($\pi = 14.91 \pm 0.75$ mas; Hipparcos Catalog), HR 4796 is three and a half times farther away than β Pic ($D = 19.3 \pm 0.2$ pc; $\pi = 51.87 \pm 0.51$ mas), but exhibits a strong IRAS excess with optical depth estimated to be twice as large (Jura 1991). An M dwarf companion is detected $7.7''$ (~ 500 AU) from the star and is believed to be physically bound on the basis of common proper motion (Jura et al. 1993). The age

of the system is estimated to be $t = 10$ Myr on the basis of isochrone fitting (Jura et al. 1998), in keeping with its identification as an outlying member of the Centaurus-Lupus association (Jura et al. 1993) with average age $t = 12-15$ Myr (de Geus, De Zeeuw, & Lub 1989). This age is younger than other well-known members of the Vega class ($t \sim 100$ Myr) and suggests that HR 4796 may be somewhat transitional between young stars ($t \sim 1$ Myr) with optically thick disks (Koerner & Sargent 1995; Mannings, Koerner, & Sargent 1997) and “Vega-type” stars (cf. Backman & Paresce 1993).

2. Observations and Results

We observed HR 4796 with JPL’s mid-infrared camera MIRLIN at the F/40 bent-Cassegrain focus of the Keck II telescope on UT 16 March 1998. MIRLIN employs a Boeing 128×128 pixel, high-flux Si:As BIB detector with a plate scale at Keck II of $0.137''$ per pixel. The latter was determined by scanning a star across both MIRLIN’s field-of-view and that of the Keck II guide camera for which the plate scale has been accurately measured. The associated field of view was $17.5''$. Background subtraction was carried out by chopping the secondary mirror at a 4 Hz rate with $8''$ throw in the north-south direction and by nodding the telescope a similar distance in the east-west direction after coadding a few hundred chop pairs. With this setup, an image of the source was always on the array; double-differenced frames were imprinted with four images of the source, two positive and two negative. These were shifted and added with the appropriate sign to make the final 64×64 ($8.3'' \times 8.3''$) images. Observations were carried out in filters centered at $\lambda = 12.5, 20.8,$ and $24.5 \mu\text{m}$ with widths 1.2, 1.7, and $0.8 \mu\text{m}$ respectively. At $12.5 \mu\text{m}$, 5 integrations of duration 18 ms were coadded at each of the chop positions and summed over 200 chop cycles before nodding. At 20.8 and $24.5 \mu\text{m}$, respectively, 5 and 3 integrations with duration 15 and 25 ms were coadded in 300 chop cycles before nodding. Small dither steps were taken between

chop-nod cycles. The infrared standards α Sco, σ Sco, and α Lyr were observed in the same way at similar airmasses. An additional sequence of images was obtained by alternating rapidly between the 12.5 and 20.8 μm filters with no telescope offsets in order to accurately determine the registration between the two wavelengths.

A two-color rendition of the combined images of HR 4796 at $\lambda = 12.5$ and 20.8 μm is displayed in Fig. 1. The underlying images are shown separately in Fig. 2a and 2b. Peak 12.5 μm emission is compact and centered on an elongated source at 20.8 μm . At $\lambda = 12.5$ μm , peak flux density of 184 ± 18 mJy is located at the position of the star and comprises nearly all of the point-like emission rising above a low-level plateau. Fainter emission accounts for an additional 40 mJy and is slightly extended to the NE and SW. We estimate the stellar photospheric emission to be 122 mJy at this wavelength by comparison with flux densities for α Lyr (Tokunaga 1998) and assuming similar temperatures and N-band magnitudes of 5.80 for HR 4796 and 0.03 for α Lyr. This implies a total excess that is nearly equal to the photospheric emission; an excess that is 50% of photospheric levels arises from very near the star. In the corresponding image at 20.8 μm , emission is elongated $\sim 3''$ at PA 30° with total flux density 1.88 ± 0.2 Jy, consistent with the 20 μm bolometer measurement of Jura et al. (1993) (1.86 Jy). Measurements at $\lambda = 24.5$ μm look roughly similar and have total flux density 2.27 ± 0.7 Jy. Surprisingly, the center of the 20.8 μm structure is not coincident with the peak emission but lies between bright peaks located at each end. Below, we interpret this morphology as arising from a nearly edge-on circumstellar disk with an inner hole and investigate its properties with the aid of a simple model.

3. Modeling and Discussion

Our measured flux densities are listed in Table I and plotted in Figure 3 together with color-corrected IRAS measurements and an upper limit obtained with the JCMT at $\lambda =$

800 μm by Jura et al. (1993). The spectral distribution of the flux densities exhibits a nearly black-body shape which peaks at $\lambda \approx 60\mu\text{m}$, well away from the maximum stellar photosphere emission. It can be reproduced by emission from a model disk with mass approximately $1.0 M_{\oplus}$, if the disk is largely devoid of radiating particles inside a radius of a few times 10 AU (Jura et al. 1995; 1998). In order to uniquely constrain the spatial distribution of dust, however, it is desirable to gain the maximum amount of information from images which resolve the circumstellar material.

The optically thin radiation from an annulus of width dr and radius r in a flat dusty circumstellar disk is estimated by Backman, Gillett, & Witteborn (1992) to be

$$f(r) = \tau_{r_0} \left(\frac{r}{r_0}\right)^{\gamma} \varepsilon_{\lambda} B[T_p(r), \lambda] \left(\frac{2\pi r dr}{D^2} sr\right) Jy,$$

where τ_{r_0} is the geometrical optical depth perpendicular to the disk plane at a fiducial radius r_0 , T_p is the particle temperature, ε_{λ} is the particle radiative efficiency relative to a black body, and D the 67 pc distance to HR 4796. For a distribution of grains with effective size, λ_0 , we assume $\varepsilon_{\lambda} = 1$ for $\lambda < \lambda_0$ and $\varepsilon_{\lambda} = (\lambda/\lambda_0)^{-1}$ for $\lambda > \lambda_0$ (see Appendix D of Backman et al. (1992) for the relation between λ_0 and a particle size distribution). The grain temperature is then $T_p(r) = 468(L_*/\lambda_0)^{0.2}(r/1\text{AU})^{-0.4}$ where L_* is the stellar luminosity in solar units. HR 4796 has a temperature similar to α Lyr with $M_V = 5.80$ at $D = 67$ pc. Then, assuming $L_* = 54 L_{\odot}$, $M_V = 0.03$, and $D = 8.1$ pc for α Lyr, we find $L_* = 18.1 L_{\odot}$ for HR 4796. Parameters which remain to be determined include λ_0 , power-law index of the optical depth γ , inner and outer radii r_{in} and r_{out} , τ_{r_0} , inclination angle ι (from face on), and position angle θ .

The morphology of the 20.8 μm emission in Fig. 1 provides a useful constraint on r_{in} , ι , θ , and τ_{r_0} under the assumption of a single power-law structure to the radial optical depth. However, it does little to constrain r_{out} , γ , and λ_0 . The latter can be better determined from fits to the flux density distribution, especially if values of the former can be derived

from a fit to the image. In both cases, we choose to evaluate the uncertainties in the range of acceptable parameter values by calculating the probability of the models given the data. We use the above formulation to simulate both the image and the flux density distribution and calculate the reduced χ^2 over the range of parameter values. The associated probability of the data given the model is taken to be $P = e^{-\chi^2}$. The probability of the model given the data is then estimated by summing and normalizing the probabilities over the whole range of parameter space considered. For the estimate of ι , individual probabilities are scaled by $\cos(\iota)$ to account for the *a priori* expectation that the system is oriented edge on (see Lay et al. 1997 for a more detailed description of this Bayesian approach).

To simulate the image of HR 4796 at $20.8\mu\text{m}$, we assumed a thin disk with emission as prescribed above, calculated the contribution at each point of an evenly-spaced 9×9 grid per pixel ($\Delta s = 1/8$ th of a pixel), and summed the result in each of 64×64 pixels corresponding to the image. A flux density corresponding to that of the stellar photosphere was added to the central pixel, and the model image was convolved with that of a standard star which was obtained at similar air mass and within a short time of the HR 4796 observations. The resulting image was then subtracted from the data and the squared difference weighted by the noise to derive reduced χ^2 and P in the usual way. Initial disk parameter values were estimated from the distribution of flux densities in order to determine orientation parameters ι and θ . The most likely values of these were then taken in a second model fit while varying r_{in} , τ_{r_0} , and γ . Assuming the best values from the latter, a repeat fit to ι and θ was completed as a check. The final results for ι and θ agreed with the initial values $\iota = 72^{+6}_{-9}^\circ$ and $\theta = 28^\circ \pm 6^\circ$.

To test for the presence and size of any clearing in the disk, we considered a range of values for γ and τ_{r_0} , since these also affect the radial distribution and intensity of emission. The value of γ was varied between 0 and -2.5; τ_{r_0} was considered over the range

$10^{-5} < \tau_{50AU} < 10$. The appearance of the $20.8 \mu\text{m}$ emission is not sensitive to increases in the choice of outer radii larger than the boundary of emission in the image, since the temperature rapidly decreases to levels at which emission is negligible at that wavelength; we adopted $r_{out} = 125 \text{ AU}$. The resulting estimate of r_{in} is evident in the plot in Fig. 4. It is clear from this figure that the source of emission in Fig. 1 cannot extend inward to within 20 AU of the star as an extrapolation of a single power-law profile to the radial optical depth. In fact, the inner radius of the disk is estimated to be a good deal larger, $r_{in} = 55 \pm 15 \text{ AU}$.

The most probable model is displayed together with the data and residuals in Fig. 2c and 2d. It is apparent that, although the presence of a hole leads to a good match with the outer disk, some emission close to the star remains in the residual image. This emission looks similar to the $12.5 \mu\text{m}$ image in appearance and may have a common origin in a warmer population of dust grains near the star with greatly decreased optical depth relative to that of the outer disk. The unresolved flux density in excess of the stellar photosphere is 62 mJy at $\lambda = 12.5 \mu\text{m}$; excess residual flux density at $\lambda = 20.8 \mu\text{m}$ is 96 mJy . These values suggest mean temperatures of $200\text{-}300 \text{ K}$ and associated distances from the star of $3\text{-}6 \text{ AU}$, depending on whether the grains are the same size as in the outer disk or radiate as black bodies. It holds in either case that the majority of grains giving rise to the emission lie well interior to the 55-AU radius of the hole and in a radial zone which corresponds to that of the Zodiacal dust in our own solar system.

The properties of the outer disk are best estimated with measurements of the emission at far infrared and millimeter wavelengths which probe cold dust (cf. Beckwith et al. 1990). Assuming an inner radius derived from our fit to the high-resolution $20.8 \mu\text{m}$ image, we try to estimate these properties with a model of the spectral distribution of flux densities. In addition to IRAS fluxes and an upper limit at $\lambda = 800 \mu\text{m}$, our measurements in narrow

bands at $\lambda = 12.5, 20.8,$ and $24.5 \mu\text{m}$ provide new constraints on the distribution of material. Our image at $12.5 \mu\text{m}$ demonstrates further that much of the infrared excess at that wavelength does *not* arise from the “disk” outside $r_{in} = 55 \text{ AU}$. Consequently, we do not attempt to fit either that measurement or the IRAS $12 \mu\text{m}$ flux density.

We varied four parameters, $\tau_{50\text{AU}}, \gamma, r_{out},$ and $\lambda_0,$ over the ranges, $10^{-5} < \tau_{50\text{AU}} < 10,$ $-4.5 < \gamma, 0, 56\text{AU} < r_{out} < 200\text{AU},$ and $10\mu\text{m} < \lambda_0 < 80\mu\text{m}$ in a fit to all flux densities at wavelengths longer than $20 \mu\text{m}$ plotted in Fig. 3. Flux from the inner region was derived from a fit to the “point-source” flux densities at 12.5 and $20.8 \mu\text{m}$ and subtracted (89, 88, 23, and 6 mJy at $24.5, 25, 60,$ and $100 \mu\text{m}$). The preferred parameter values are $r_{out} \approx 55 - 80 \text{ AU}$ and $\lambda_0 \approx 10 - 40\mu\text{m};$ $\tau_{50\text{AU}}$ and γ are not well determined within these ranges. Unless maintained by some orbiting body, an extremely narrow ring is probably too short-lived to be likely. Consequently, we assume $r_{out} = 80 \text{ AU}$ for the model plotted in Fig. 3, together with $r_{in} = 55 \text{ AU}, r_{out} = 80 \text{ AU}, \lambda_0 = 30 \mu\text{m}, \tau_{50\text{AU}} = 0.065$ and $\gamma = -2.0.$

These observations provide direct evidence for the existence of a disk around the young A0 star, HR 4796, with size and orientation that agree with the results of an independent discovery (Jayawardhana et al. 1998). Further, the morphology of emission at $\lambda = 20.8 \mu\text{m}$ reveals an inner hole in the disk with radius $55 \pm 15 \text{ AU}$. Emission in excess above the photosphere at $12.5 \mu\text{m}$ arises predominantly from a region interior to this radius. When compared to excess $20.8 \mu\text{m}$ emission at this location, the $12.5 \mu\text{m}$ radiation yields a source temperature of a few hundred K, corresponding to a radial distance of a few AU from the central star. The outer and inner components of the dust distribution are analogous, respectively, to the Kuiper Belt and Zodiacal components of dust within our own solar system. Taken together, these properties are startlingly like those believed to have existed in the late bombardment stage of the early solar system, when collisions between cometesimals in the outer solar system and between planetesimals or asteroids in a

terrestrial planet-forming zone were likely to have generated a large population of smaller dust grains distributed in much the same way as those around HR 4796.

We wish to thank Robert Goodrich, operator assistants Ron Quick and Joel Aycock, and the W.M. Keck Observatory (WMKO) summit staff for helping to adapt and operate MIRLIN at the Keck II visitor instrument port. Our heart-felt thanks extend especially to director F. Chaffee for supporting the use of MIRLIN at WMKO. We are also indebted to M. Jura for many helpful discussions and to R. Jayawardhana and L. Hartmann for sharing results prior to publication. Development of MIRLIN was supported by the JPL Director's Discretionary Fund and by an SR+T award from NASA's Office of Space Science. The use of MIRLIN at the Keck Observatory was supported by an award from NASA's Origins program. Portions of this work were carried out at the Jet Propulsion Laboratory, California Institute of Technology, under contract with the National Aeronautics and Space Administration. Data presented herein were obtained at WMKO, which is operated as a scientific partnership between Caltech, University of California, and NASA, and was made possible by the generous financial support of the W.M. Keck Foundation.

REFERENCES

- Backman, D.E., Gillett, F.C., & Witteborn, F.C., 1992, *ApJ*, 385, 670
- Backman, D.E., & Paresce, F., 1993, in *Protostars and Planets III*, (ed. E.H. Levy and J.I. Lunine), Tucson: University of Arizona Press, p. 1253
- de Geus, E.J., de Zeeuw, P.T., & Lub, J., 1989, *A&A*, 216, 44
- Houk, N., 1982, in *Michigan Spectral Catalog* (Ann Arbor: Univ. of Michigan Press), p. 3
- Jayawardhana, R., Telesco, C., Fazio, G., Hartmann, L., Pena, R., Fisher, S., 1998, *ApJ* submitted.
- Jura, M., 1991, *ApJ*, 383, L79
- Jura, M., Zuckerman, B., Becklin, E.E., & Smith, R.C. 1993, *ApJ*, 418, L37
- Jura, M., Ghez, A.M., White, R. J., McCarthy, D.W., Smith, R.C., & Martin, P.G., 1995, *ApJ*, 445, 451
- Jura, M., Malkan, M., White, R., Telesco, C., Pena, & Fisher, R.W. 1998, *ApJ*, in press.
- Kalas, P., & Jewitt, D., 1995, *Ap&SS*, 223, 167
- Kalas, P., & Jewitt, D., 1996, *AJ*, 111, 1347
- Koerner, D.W., & Sargent, A.I., 1995, *AJ*, 109, 2138
- Lagage, P.O., & Pantin, E., 1994, *Nature*, 369, 628
- Lay, O.P., Carlstrom, J.E., & Hills, R.E. 1997, *ApJ*, 489, 917
- Mannings, V., Koerner, D.W., & Sargent, A.I., 1997, *Nature*, 388, 555
- Pantin, E., Lagage, P.O., & Artymowicz, P., 1997, *A&A*, 327, 1123
- Smith, B.A., Fountain, J.W., & Terrile R.J., 1992, *A&A*, 261, 499
- Smith, B.A., & Terrile R.J., 1984, *Science*, 226, 4681

Stauffer, J.R., Hartmann, L.W., & Barrado y Navascues, D., 1995, *ApJ*, 454, 910

Tokunaga, A., 1998, in *Astrophysical Quantities*, (ed. Cox), London: Dover, in press.

Fig. 1.— Composite 2-color image of the emission from HR 4796 at $\lambda = 12.5$ (cyan) and $20.8 \mu\text{m}$ (red). Registration was accomplished by taking images at the same telescope position and rapidly cycling between both filters.

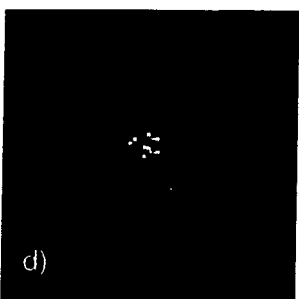
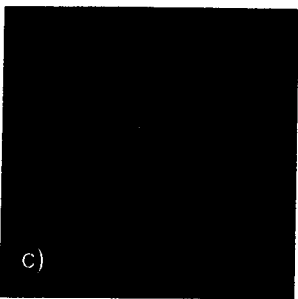
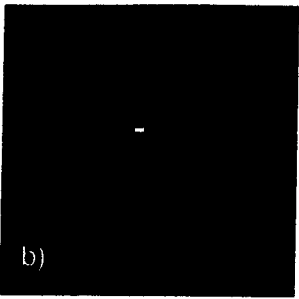
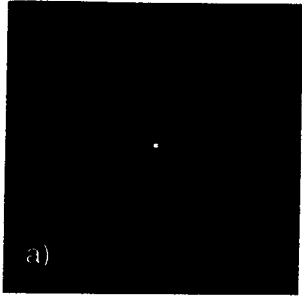
Fig. 2.— a) Image of the intensity of emission from HR 4796 at $\lambda = 12.5$. b) As in a, but at $20.8 \mu\text{m}$. c) Model of the $20.8 \mu\text{m}$ emission from a flat dusty disk with a 55 AU inner hole and a central star with flux density matched to that of HR 4796. The model was generated as described in the text and convolved with a PSF derived from a standard star. d) Residuals from the subtraction of the model from the image with exaggerated intensity scale. Excess $20.8 \mu\text{m}$ emission near the star has a flux density of 96 mJy.

Fig. 3.— Plot of the flux densities for HR 4796 listed in Table I. The solid curve marks the total emission from the stellar photosphere (dashed line) and a model of the emission from a disk with 55 AU inner hole (dotted line).

Fig. 4.— Plot of the probability distribution for values of the radius of an inner hole in the disk. As described in the text, the radial power-law index of the geometric optical depth was also varied from $\gamma = -2.5$ to 0.0 . The distribution over all values of γ is shown as a solid line. That for $\gamma = 0.0$ is plotted as a dashed and dotted line, and for $\gamma = -2.5$ as a dotted line.

Table 1. Flux Densities for HR 4796

λ_{eff} (μm)	$\delta\lambda$ (μm)	Flux Density (Jy)	Uncertainty (Jy)	Photosphere (Jy)	Excess (Jy)
12.5	1.2	0.223	0.018	0.122	0.101±0.018
20.8	1.7	1.880	0.170	0.047	1.813±0.170
24.5	0.8	2.270	0.700	0.033	1.994±0.700
12.0	6.5	0.309	0.028	0.136	0.173±0.028
25.0	11.0	3.280	0.13	0.032	3.250±0.130
60.0	40.0	8.640	0.43	0.006	8.630±0.430
100.0	37.0	4.300	0.34	0.002	4.300± 0.340
800.0	100.0	< 0.028	-	-	-



Size of Inner Hole

